A "Phoenix" Reflectarray Unit Cell with Reduced Size and Inductive Loading

Tony Makdissy [1*], Raphaël Gillard [1], Erwan Fourn [1], Miguel Ferrando-Rocher [1], Etienne Girard [2], Hervé Legay [2], Laurent Le Coq [3]

[1] Institute of Electronics and Telecommunications of Rennes (IETR), INSA, UMR CNRS 6164, 35708 Rennes, France
[2] Research and Development Department, Thales Alenia Space, 31037 Toulouse, France
[3] Institute of Electronics and Telecommunications of Rennes (IETR), University of Rennes 1, UMR CNRS 6164, 35042 Rennes, France
[*]tony.makdissy@gmail.com

Abstract: This paper presents a new Phoenix unit cell with reduced size ($\lambda_0/3$ at centre frequency). Three different techniques are investigated to preserve a complete 360° phase range, with quasi-linear and parallel phase responses over a reasonable frequency band, in spite of this small size. The phase cycle successively uses two different printed elements with complementary capacitive and inductive responses. The studied techniques aim at increasing the insufficient inductive effect. As a demonstration, a 1877-element reflectarray is fabricated with the technique compatible with a single-substrate fabrication process. Measured results show a 1-dB gain bandwidth of 11.3%.

1. Introduction

Reflectarrays [1] have experienced strong development in the past two decades. This kind of antennas has the potential to form complex radiation patterns with relative simplicity, low cost, low losses and low profile [2].

It is well known that the bandwidth of a passive reflectarray antenna mainly depends on the bandwidth of the phase-shifting cell and on the geometry of the antenna [3], [4]. Thus, while designing a reflectarray, one of the main challenges is to design a unit cell which provides a quasi-linear phase variation versus frequency over a complete 360° range. Another critical point to be considered is the smoothness of the cell evolution over the phase cycle. Indeed, it has been shown theoretically in [5] that strong geometric variations between two consecutive cells introduce a significant uncertainty in the simulated phase (that usually relies on a local periodicity assumption). The negative effect of such transitions has been shown experimentally at the array level in [6]. Therefore, there is definitively a big interest to provide a very smooth geometry evolution of the cell on the surface of the array, even at phase transitions, after a complete 360° cycle.

Multilayer solutions improve the phase range of the unit cell and its bandwidth. Some of them use stacked patches on a multilayer substrate such as the solutions proposed by Encinar [7], [8]. Other ones involve true-time delay (TTD) elements [9].

Chaharmir proposed an alternative technique with relative simplicity and low cost. It consists in using multiple resonators printed on a single layer substrate [10]-[12]. The phase range easily reaches 360° with a wide bandwidth. Recently, several derived topologies have been proposed [13], [14] also showing good performance. The main drawback of these solutions is the quite large cell size ($0.43\lambda_0$ - $0.5\lambda_0$).

The so-called "Phoenix" cell is another solution whose main interest is to avoid ruptures in the periodicity of the reflectarray layout, due to its unique capability to loop back to the initial geometry after a 360° cycle [15]. The phase variation is quasi-linear since the cell combines two concentric annular slots of complementary size. Moreover, it has been demonstrated that this kind of cell can be used to produce contoured beams for space communications [6]. However, in its initial version, the "Phoenix" cell size was quite large ($0.66\lambda_0$).

Several studies have demonstrated the interest of using sub-wavelength elements [16]-[19] or miniaturised-element frequency selective surfaces (MEFSS) [20] in order to improve bandwidth further. On the other hand, reducing the size of the unit-cell reduces the phase range it can provide. In [21], we proposed an alternative "Phoenix" cycle (also looping back to its initial state) offering a smaller lattice ($0.42\lambda_0$ at 12.5 GHz). It is based on the combination of a patch and a slot (both used out of resonance) in the same phase cycle. A large frequency band with quasi-linear phase responses was demonstrated. However, the achieved phase range was only 330°.

In this paper, the same cycle is considered but the size of the unit-cell is reduced further (down to $\lambda_0/3$). Moreover, three different techniques are presented and discussed in order to complete the phase range up to 360° while preserving quasi-linear phase responses over a reasonable bandwidth, in spite of the limited cell size. Equivalent circuits are provided for all techniques, highlighting the different involved physical mechanisms. Finally, the last technique is selected for the fabrication of a prototype array, since it is fully compatible with a single-layer fabrication process.

2. Initial Performances of the New “Phoenix” Cycle

As described in [21], the proposed cycle involves two different elements successively: first a metallic cross with a capacitive behaviour and then a metallic grid (defining square apertures) with an inductive behaviour. The first part of the cycle consists in growing two crossed dipoles of size $2w$ (see Fig. 1(a)) until crosses in successive cells touch each other and form a metallic grid. The second part of the cycle then consists in narrowing the width w of the metallic grid (see Fig.1 (b)), which increases the size of the defined square apertures. The cycle ends with the complete vanishing of the metallization before the

cross is grown again. Note that the proposed cell is suitable to operate in dual linear polarization (with identical coverage for both polarizations).

In this new study, we have considered a phase-shifting cell of size $Lc=8mm$ ($\lambda_0/3$ at 12.5GHz). It is printed on a 3.175mm thick Duroïd substrate ($\varepsilon_r=2.17$) and backed by a metallic ground plane. In order to assess the performance of the cell, electromagnetic simulations using HFSS® commercial software have been carried out. The cell is assumed to be placed in an infinite array of identical elements and illuminated with a plane wave under normal incidence. Fig. 2 shows the reflected phase versus frequency for different values of w within the cycle. The different phase responses are almost linear and parallel. The cross mainly operates as a capacitance and the grid as an inductance, both elements providing complementary phase ranges [21]. Finally, the maximum frequency dispersion is 36°/GHz at 10.5GHz but the overall phase range is only 305°. Indeed, Fig. 2 clearly shows that the inductive effect brought by the narrowest metallic grid ($w=0.15mm$ as imposed by technological constraints) is not sufficient to bridge the 55° gap between inductive cells (in blue) and capacitive ones (in red), while the capacitive sub-range is totally covered with the crossed dipoles. This is confirmed by circuit simulations performed using ADS® commercial software. In these simulations, the metallic cross is replaced by a pure capacitance and the metallic grid by a pure inductance. These elements are loaded with a short-circuited transmission line representing the substrate backed by ground plane. An equivalent circuit is given in Fig. 3(a) where the admittance $Y=jB$ stands for the reactive element (either capacitive or inductive) while l is the substrate thickness. Fig. 3(b) shows that the maximum inductance necessary to complete the phase cycle is approximately 80nH when the maximum inductance permitted by the grid (for w=0.15 mm) is only 5.34nH. In the following section, solutions for enhancing the inductive effect will be investigated.

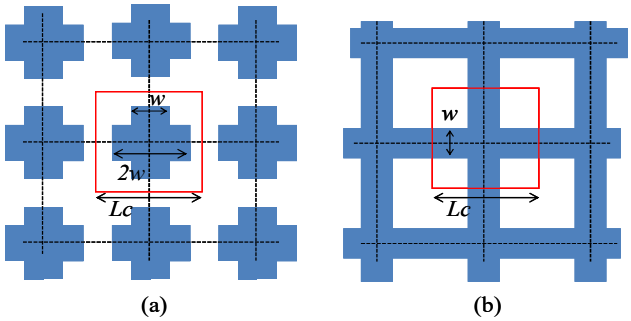

Fig. 1. *Phase-shifting cell (inside the red square) based on*
a crossed dipoles
b metallic grid (square apertures)

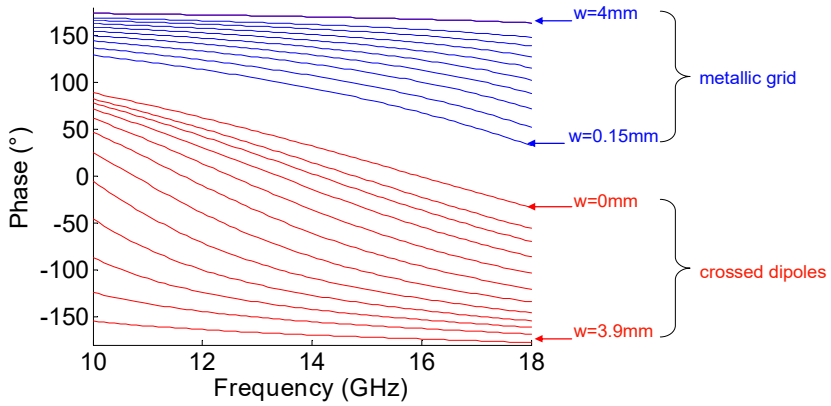

Fig. 2. *Reflected phase versus frequency for different values of w within the cycle*

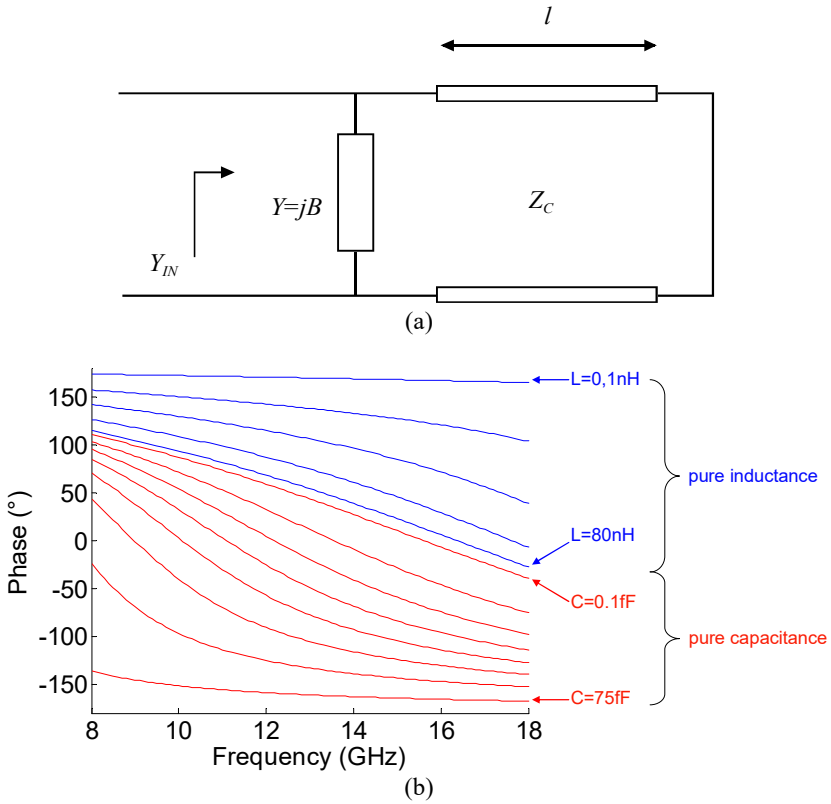

Fig. 3. *Ideal performance of a phase-shifting cell*
a Equivalent circuit of a reflectarray cell composed of a pure reactive element above a ground plane
b Ideal reflected phase versus frequency for different values of the pure capacitance C and the pure inductance L

3. Enhancement of the Inductive Effect in the Proposed "Phoenix" Cycle

Three different solutions are considered to increase the maximum achievable inductance.

3.1. Moving the Grid Towards Ground Plane

A first possible solution is to move the thinnest grid towards the ground plane for elements requiring a large inductance. We note that the capacitive element, the cross, is maintained at a fixed distance above the ground plane regardless its size *w*.

Fig. 4(a) shows a typical configuration where the inductive element is located at a distance *x* from the ground. The reference plane for the definition of the reflected phase is kept at the initial distance *l* because most elements in the reflectarray will be printed in this plane. The input impedance Z_{IN} is then given by

$$Z_{IN} = jZ_C \frac{L\omega\left(1+t_x^2\right)+Z_C t_x - Z_C \frac{t_x^2}{t_l}}{Z_C t_x^2 + Z_C \frac{t_x}{t_l} + L\omega \frac{\left(1+t_x^2\right)}{t_l}} \tag{1}$$

with t_x=tanβx and t_l=tanβl.

For the sake of simplicity, calculations will be carried out in the specific case where $l=\lambda/4$. In practice, the situation may be slightly different but we will show with simulations that the observed effect is preserved anyway. In this case, we have $t_l=\infty$ and (1) is reduced to:

$$Z_{IN} = j\frac{L\omega\left(1+t_x^2\right)+Z_C t_x}{t_x^2} \tag{2}$$

When *x* gets very small, t_x tends to 0 and (2) can be approximated by a pure inductive impedance as:

$$Z_{IN} = jL_{eq}(x)\omega \tag{3}$$

with

$$L_{eq}(x) \approx \frac{L}{t_x^2} \tag{4}$$

which shows the synthesized inductance L_{eq} can be made as large as desired, provided the grid is moved close enough to the ground plane.

In order to evaluate the feasibility of this technique, simulations have been carried out using HFSS® with the same conditions as in section 2 (*Lc=8mm*, *l=3.175mm*, i.e. Lc= $\lambda/3$ and $l\approx\lambda/5$ at 12.5GHz) (see Fig. 4(b)). Fig. 4(c) clearly shows the satisfactory behaviour of the cycle. Indeed, shifting the narrowest metallic grid (*w=0.15mm*) in the substrate up to 0.175mm above the ground plane permits to bridge the

initial 55° gap continuously all over the frequency band. Moreover, 36°/GHz is still the maximum frequency dispersion at 10.5GHz. However, this first solution is not simple to implement practically as it requires the metallization have to be printed at different levels.

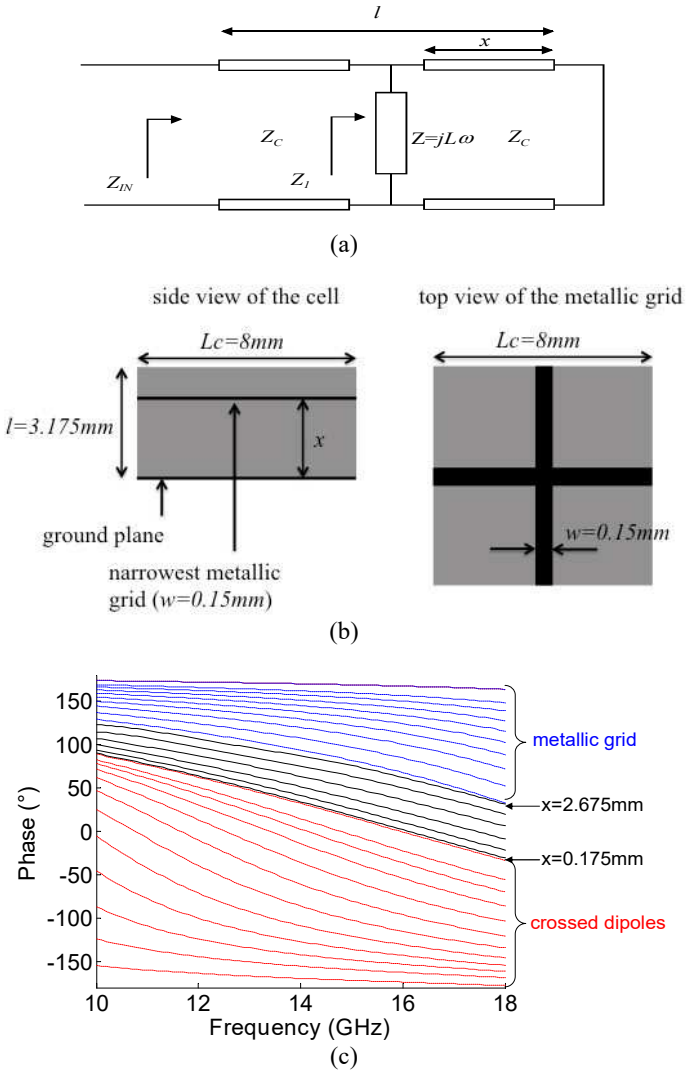

Fig. 4. *Simulated performance of a phase-shifting cell where the reactive element (here an inductive element) is moved towards the ground plane*
a Equivalent circuit of the reflectarray cell
b Unit cell with the narrowest metallic grid shifted towards ground plane
c Complete phase range provided by the reflectarray cell

3.2. Using a Capacitive Loading of the Ground Plane

A second solution to complete the 360° phase range could be a capacitive loading of the ground plane. The capacitive loading of the ground can be provided by square apertures of size *t* (see Fig. 5(a)-(b)). In practice, in order to prevent from any losses through these apertures, a second ground plane has to be placed *λ/4* behind the capacitive one (see Fig.5(a)-(c)).

Let us assume the ground plane backing the cell at distance l is replaced by a reactive impedance $Z=jX$ (see Fig. 6(a)). We also consider the usual printed element itself has been suppressed, which means the reflective phase is only controlled by the reactive loading of the ground plane.

The input impedance Z_{IN} at the reference plane is:

$$Z_{IN} = Z_C \frac{jX + jZ_C \tan \beta l}{Z_C - X \tan \beta l} \tag{5}$$

assuming $l=\lambda/4$, it becomes:

$$Z_{IN} = jZ_C^2 B \tag{6}$$

where X is expressed as $X=-1/B$.

Clearly, a large inductive effect can be obtained by loading the ground with a large capacitance (large $B=C\omega$).

In this solution, the capacitive loading of the ground plane is used without any printed element (neither cross, nor metallic grid) on the top of the cell. Simulations (once again with $l=3.175mm$) show that decreasing the size of the apertures permits to complete the 360° of phase range at 12.5GHz (see Fig.6 (b)). The smallest required aperture is $t=0.1mm$ which results in a 0.2mm of separation between two capacitive patches, which is fully compatible with the fabrication restriction. Here also the maximum frequency dispersion of the phase is 36°/GHz at 10.5GHz. Once again, this solution requires several metallization levels (only two here), which makes the technological process more complex than the initial one. Moreover, it is less attractive than the previous one for the upper part of the frequency band.

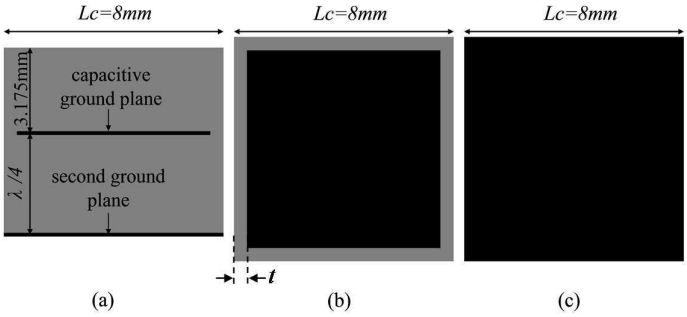

Fig. 5. *Capacitive loading of the ground plane*
a side view of the cell
b top view of the capacitive ground plane
c top view of the full ground plane behind the capacitive one

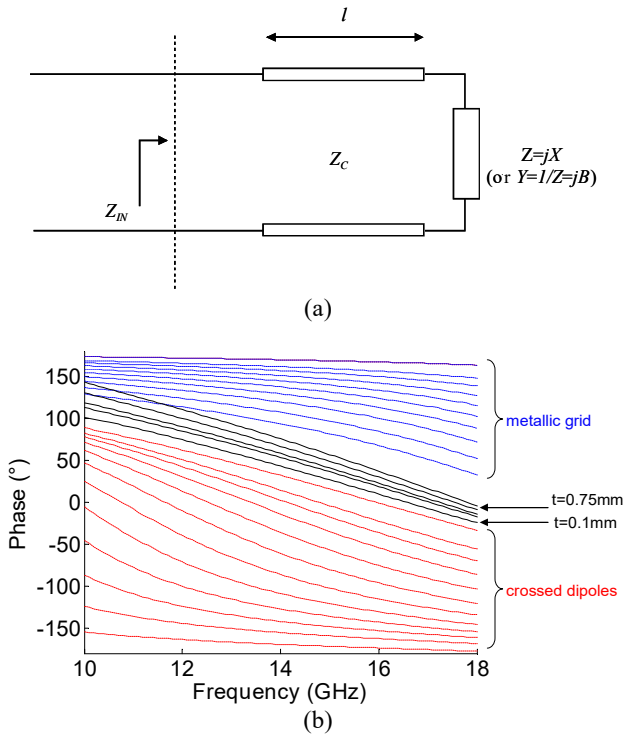

Fig. 6. *Simulated performance of a phase-shifting cell with a capacitive loading of the ground plane*
a Equivalent circuit of the reflectarray cell
b Complete phase range provided by the reflectarray cell

3.3. Using a "Meandered" grid

A third solution to increase the phase range consists in introducing a meander in the narrowest metallic grid (*w=0.15mm*). As shown in Fig.7 (a), meanders are introduced in *x*-directed and *y*-directed strips in order to preserve dual linear polarization. In the following, only the *y*-polarized electric field is considered. The reasoning is the same for the orthogonal polarization.

Due to the meander, a shunt capacitance is added to the initial grid inductance (see Fig.7 (b)): it accounts for the increased coupling between the *x*-directed metallic strips. The additional series inductance, due to the meanders in the *y*-directed strips, is quite negligible, as it will be shown later. The equivalent impedance of the grid is then a shunt resonator (see Fig.7 (b)).

Assuming that the cell is located *λ/4* above the ground plane, the input impedance is given by:

$$Z_{IN} = j\frac{L\omega}{1-\left(\frac{\omega}{\omega_0}\right)^2} \tag{7}$$

with:

$$\omega_0 = \frac{1}{\sqrt{LC}} \tag{8}$$

where L is the global inductance of the y-directed strips and C represents the capacitive coupling between the x-directed strips.

If ω is kept below ω_0, the global inductance can be increased and we obtain an equivalent inductance given by:

$$L_{eq} = \frac{L}{1-\left(\frac{\omega}{\omega_0}\right)^2} \tag{9}$$

So this is clearly another solution to obtain the expected high inductive effect that is necessary to complete the cycle. The advantage is that this effect can be obtained without using any additional metallization levels.

Simulations (with *l=3.175mm*) show that increasing the length m of the meander from 3mm to 5.5mm is sufficient to complete the phase range at 12.5GHz (see Fig. 7(c)). However, contrary to the first technique (moving the grid towards the ground), the frequency dispersion of the phase increases with m. It is larger than the previous maximum dispersion (36°/GHz) for *m>5mm* and reaches 45°/GHz (at 15GHz) for *m=5.5mm*, at the expense of the parallelism of the phase responses.

Moreover, Fig. 7(d) shows that, for a particular element size, the maximum variation of the reflected phase is 100° between 11GHz and 15GHz. This means that an average frequency dispersion of 25°/GHz is obtained over 30% of bandwidth. This seems to be better than the performance of the original "Phoenix" cycle [15] where the average frequency dispersion is 25°/GHz over 25% of bandwidth (14-18GHz). We note that this comparison is only indicative since both the cell sizes and central frequencies are different.

The increase in the frequency dispersion with the meanders can be explained easily based on the equivalent circuit. Indeed, a deeper insight at the equivalent inductances L_{eq} in (4) and (9) shows that the involved mechanisms are different. Clearly, (9) involves a resonant mechanism that makes the cell more dispersive. Thus, the desired increase in the inductive effect can only be obtained if we approach the resonance.

In order to assess the values of the inductance L and capacitance C of the LC shunt resonator of the thinnest grid with meanders, the unit cell was first simulated using HFSS® commercial software (for different size for the meander) with two ports: Port 1 above the cell (representing the initial excitation), and port 2 replacing the ground plane. With this simulation, the admittance matrix of the element is computed. Then, this matrix is exported into Keysight Technologies (Agilent) commercial circuit simulator ADS®, where the equivalent LC circuit is synthesized [21]. The values of the inductance L and

capacitance C of the grid with meanders are calculated and summarized in Table 1 for a y-polarized electric field. As the length of the meander is increased, the inductance L remains almost constant, and the capacitance C increases. We note that the calculation of the values of L and C is limited to a meander length $m=4.5mm$ since for greater values, coupling phenomena appear between the orthogonal meanders making the analysis of the circuit more complex.

Finally, meanders with $m>5mm$ are only required on a very limited number of cells (those requiring the larger inductive effect). Moreover, this technique has the unique property to be compatible with a single-layer fabrication process. Therefore, it has been selected in order to conduct an experimental validation on an antenna demonstrator.

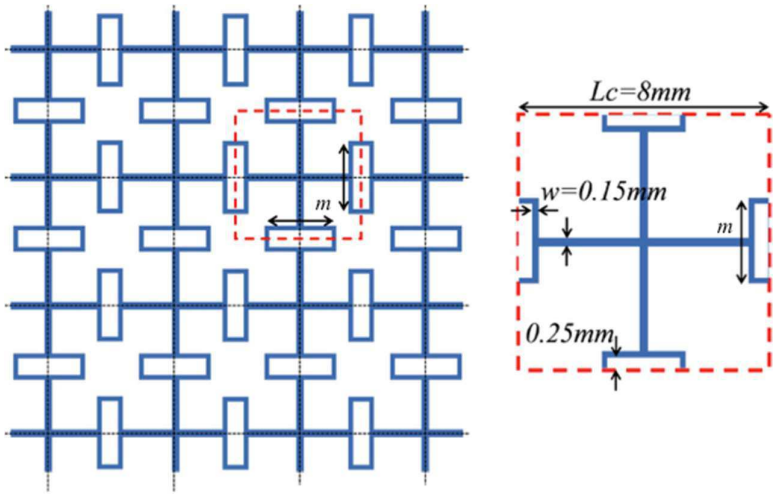

(a)

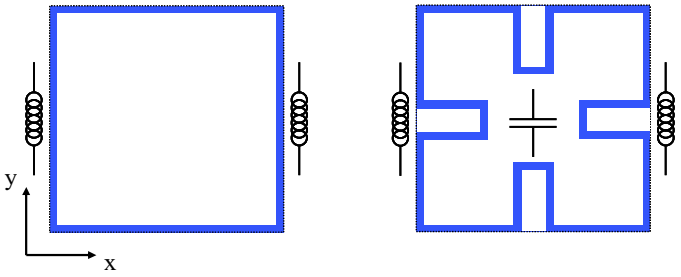

(b)

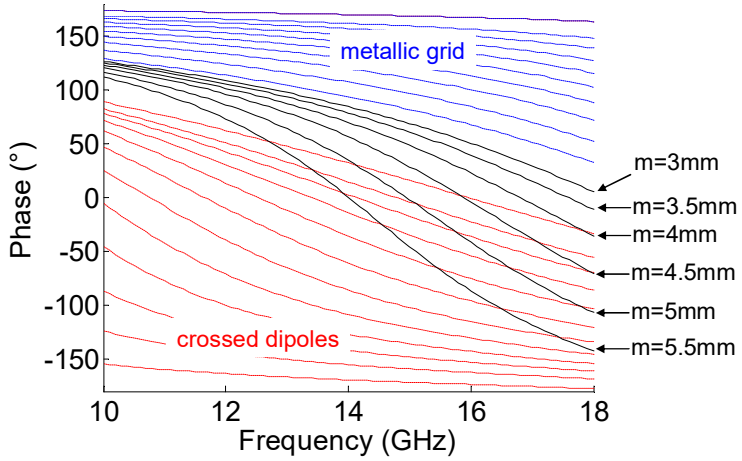

(c)

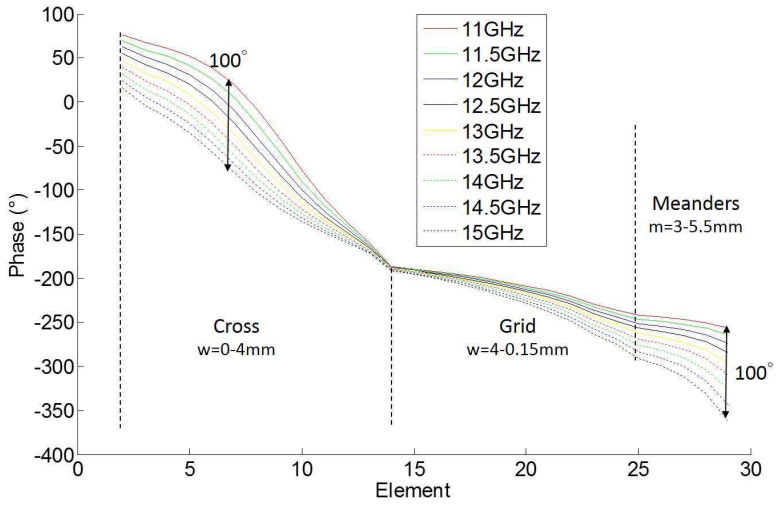

(d)

Fig. 7. *Simulated performance of a phase-shifting cell with a "Meandered" grid*
a Metallic grid and unit cell with meanders of variable length m
b Equivalent reactive effect of a simple grid and of a grid with meander for y-polarization
c Complete phase range provided by the reflectarray cell
d Phase variation over the complete cycle for different frequencies

Table 1 Values of *L* and *C* in the *LC* shunt resonator of the grid with meanders

m (mm)	L (nH)	C (fF)
3	5.25	4.9
3.5	5.31	6.5
4	5.35	8.5
4.5	5.39	11

4. Behavior of the New "Phoenix" Cycle Under Oblique Angle of Incidence

The proposed cycle with the meanders is now studied by placing the cell in an infinite periodic array illuminated with a plane wave under oblique incidence. The oblique angle of incidence results in resonances (not shown) in the phase responses at frequencies below 12GHz and above 15GHz. Then, the available bandwidth has to be reduced to 12-15GHz where the frequency dispersion is maintained below 45°/GHz. As an illustration, the phase responses of the complete cycle, along x and along y, for the particular angle of incidence ($\theta=30°$, $\varphi=60°$), are illustrated in Fig. 8. The phase range provided at 13.5GHz (centre of the reduced band) is 360°. The maximum frequency dispersion at 13.5GHz is 34°/GHz for x-polarization and 30°/GHz for y-polarization.

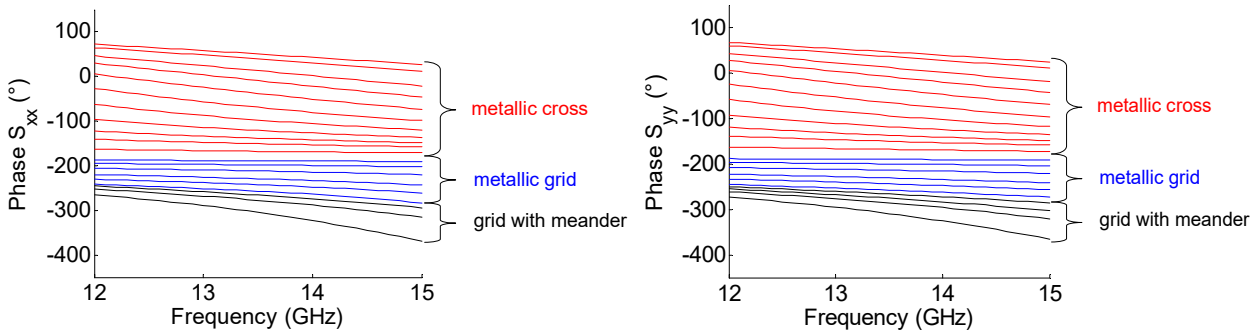

Fig. 8. *Phase responses of the complete cycle (with meanders) for an oblique incidence ($\theta=30°$, $\varphi=60°$)*
a for x-polarization
b for y-polarization

5. Experimental Results

A 1877-element offset fed circular reflectarray was designed, fabricated and measured. The diameter of the antenna is 400mm. The primary source is a dual linear polarization small size horn antenna operating in the band 12-18GHz. Its phase center is located 8mm inwards the aperture. It is positioned 607mm above the centre of the array (see Fig. 9(a)). A 21.5° offset is used to limit feed blockage. The maximum angle of incidence is 37° and the maximum tapering is -5dB at the edge of the array. The latter was designed based on phase-only synthesis for broadside radiation at 13.5GHz. Globally, this configuration can be seen as a worst case because of the non-specular main beam direction and the non-optimal aperture illumination, which results in a limited bandwidth and reduced antenna efficiency, as it will be observed hereafter. This experimental setup (poor illumination and non-specular main beam) was selected based on the possibility of reuse of an available antenna support, and not to obtain the optimal performance.

Only 72 elements (3.8% of elements) in the array include meanders with $m>5mm$. A photograph of the fabricated prototype inside the anechoic chamber is illustrated in Fig. 9(b). Fig. 10 illustrates the

normalized radiation patterns, measured at 13.5GHz (centre of the frequency band), in E plane and H plane for both polarizations. It shows that the side lobes levels (SLL) are less than -18dB and the cross polarizations are below -20dB. Due to the offset fed configuration, the illumination is not symmetrical in the *y0z* plane. This results in specular reflection in this plane (E plane in *y*-polarization and H plane in *x*-polarization). However, this reflection remains below -20dB. The main beam, expected to be pointed along +*z* direction, is shifted by 1° in *x0z* plane and by 0.7° in *y0z* plane. This is due to uncertainties in the position and orientation of the horn. The half power beamwidth of the main lobe is about 3.4°.

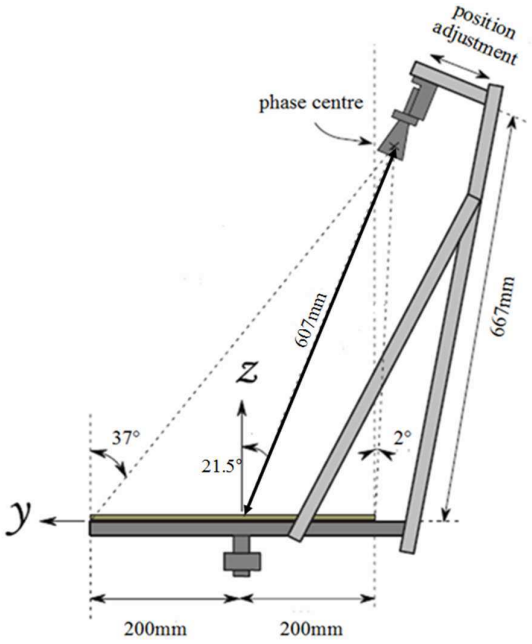

(a)

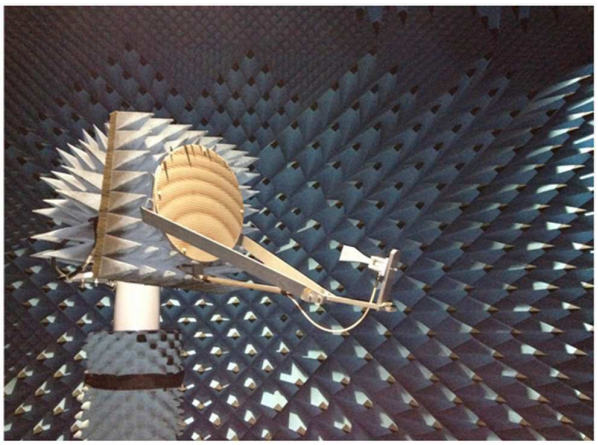

(b)

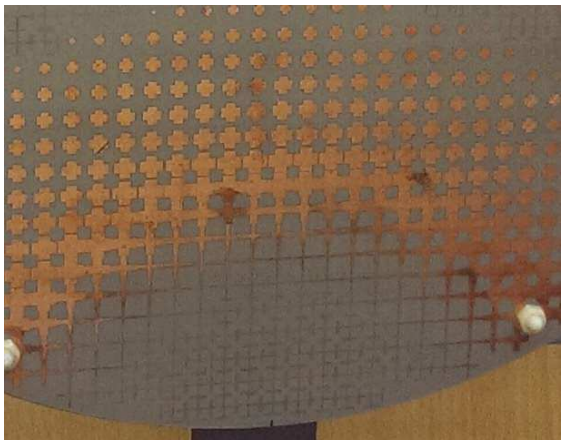

(c)

Fig. 9. *Fabricated antenna*
a Dimensions of the antenna support
b Photograph of the fabricated prototype inside the anechoic chamber
c Photograph of the complete cycle on the fabricated prototype

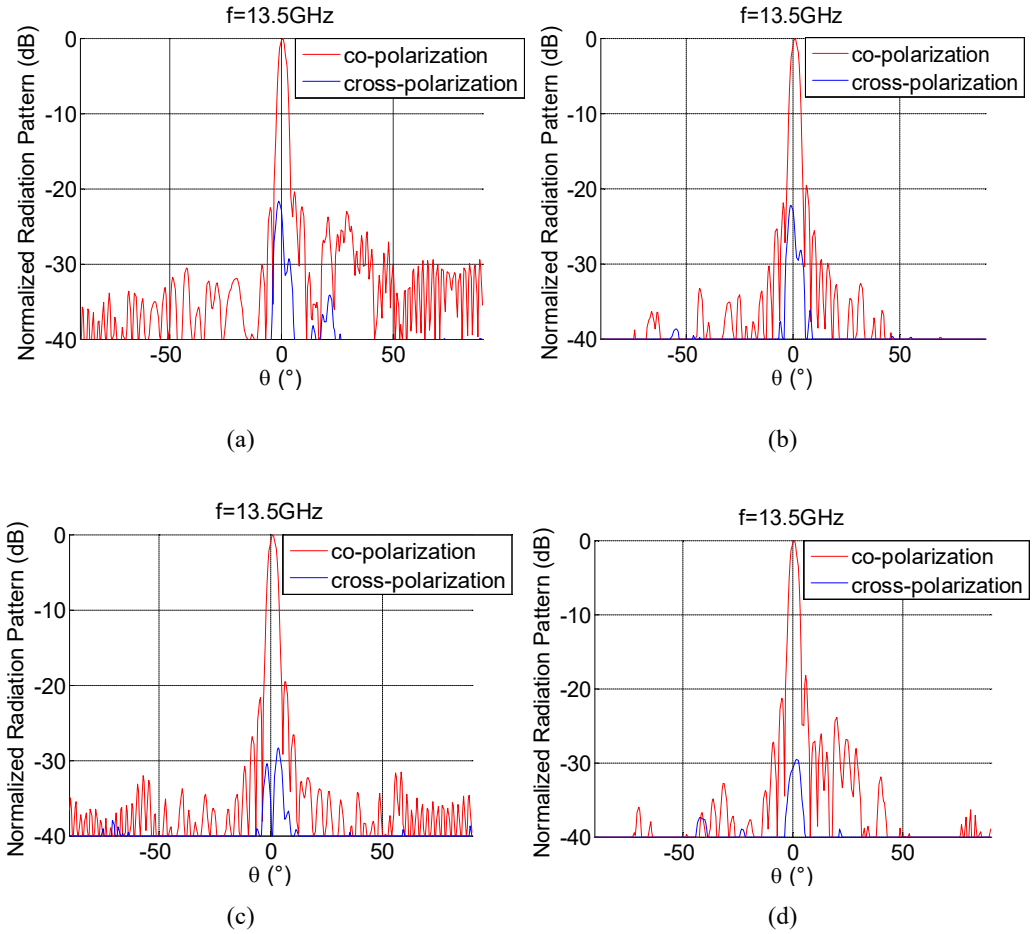

Fig. 10. *Normalized radiation pattern measured at 13.5GHz*
a E plane when the electric field is y-polarized (vertical polarization)
b H plane when the electric field is y-polarized (vertical polarization)
c E plane when the electric field is x-polarized (horizontal polarization)
d H plane when the electric field is x-polarized (horizontal polarization)

Fig. 11 shows the variation of the radiation pattern with frequency in *y0z* and *x0z* planes. When the electric field is *y*-polarized, the SLL and the cross polarization level of the radiation pattern in the E plane are maintained respectively 18dB and 20dB below the main beam in the 12.5-14 GHz band (see Fig. 11(a)). This reduced frequency band corresponds to the 1-dB gain bandwidth as it will be shown hereafter. The direction of the main beam varies with frequency from -1° to 1.5°. The same behaviour is obtained in the H plane for the *x*-polarization (see Fig. 11(b)). When the electric field is *y*-polarized, the SLL and the cross polarization level of the radiation pattern in the H plane are maintained respectively 17dB and 20dB below the main beam in the 12.5-14 GHz band (see Fig. 11(c)). Moreover, the main beam direction is tilted by 1°. The same behaviour is obtained in the E plane for the *x*-polarization (see Fig. 11(d)).

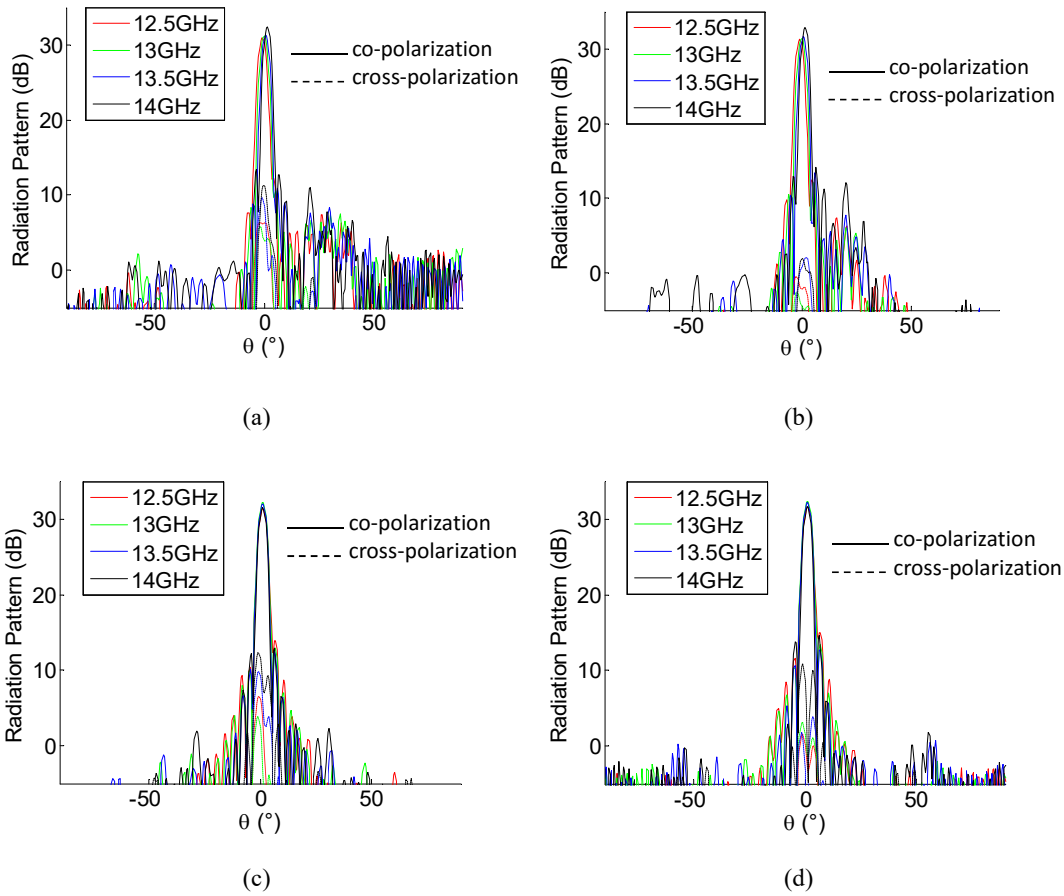

Fig. 11. *Radiation pattern measured for different frequencies*
a *y*-polarization, E plane
b *x*-polarization, H plane
c *y*-polarization, H plane
d *x*-polarization, E plane.

The gain was measured at +*z* direction in both polarizations (see Fig. 12). A maximum gain is obtained at 13.25GHz. It is equal to 31.5dBi and 31.3dBi for *x*-polarization and *y*-polarization respectively. This is equivalent to 45% of antenna efficiency. Such a quite small value may be explained by the non-optimal illumination of the reflecting panel in this canonical breadboard (-5dB of tapering at the edge of the array). The 1-dB gain bandwidth is 11.3% from 12.5GHz to 14GHz. Bandwidth could certainly be improved further using a configuration where the main beam is steered in the direction of specular reflection.

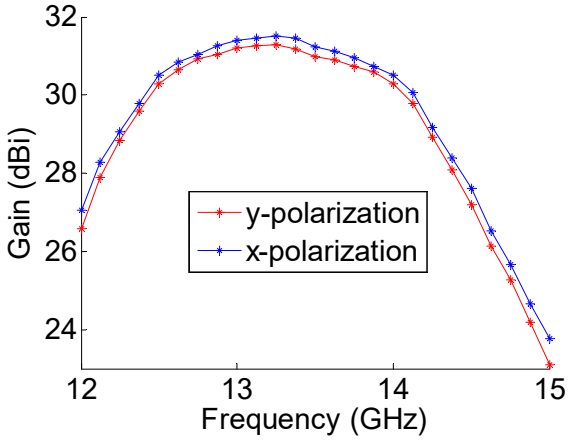

Fig. 12. *Gain versus frequency in both polarizations*

6. Conclusion

In this paper, a new sub-wavelength "Phoenix" cell is proposed. It combines two different elements used out of their resonance in order to provide a wide bandwidth. The initial cell is not able to provide a 360° of phase range. In order to overcome this limitation, three different techniques were proposed. The third one is fully compatible with a single-layer manufacturing process. These techniques were analyzed based on equivalent electric circuits supported with simulations. They showed that a complete 360° phase range with quasi-linear and parallel phase responses over a reasonable frequency band can be obtained in spite of the small size of the cell. Finally a reflectarray prototype using the technique with the simpler technological process was fabricated and measured. In spite of the non-optimal antenna configuration, a 1-dB gain bandwidth of 11.3% was demonstrated and quite good performance in term of radiation pattern was obtained.

7. References

[1] J. Huang, J. A. Encinar: 'Reflectarray Antennas', Wiley-IEEE Press, ISBN: 978-0-470-08491-5, November 2007.
[2] D. M. Pozar, S. D. Targonski, and R. Pokuls: 'A shaped-beam microstrip patch reflectarray', IEEE Transactions on Antennas and Propagation, vol. 47, no. 7, July 1999, pp. 1167–1173.
[3] D. M. Pozar: 'Bandwidth of reflectarrays', Electronics Letters, vol. 39, no. 21, October 2003, pp. 1490-1491.
[4] M. E. Bialkowski and K. H. Sayidmarie: 'Bandwidth considerations for a microstrip reflectarray', Progress in Electromagnetics Research B, vol. 3, 2008, pp. 173-187.
[5] M-A. Milon, R. Gillard, H. Legay: 'Rigorous analysis of the reflectarray radiating elements: Characterization of the specular reflection effect and the mutual coupling effect', 29th ESA workshop on Multiple Beams and Reconfigurable Antennas, Netherlands, April 18-20, 2007.
[6] H. Legay, D. Bresciani, E. Labiole, et al.: 'A multifacets composite panel reflectarray antenna for a space contoured beam antenna in ku band', Progress In Electromagnetics Research B, vol. 54, 2013, pp. 1–26.
[7] J. A. Encinar: 'Design of Two-Layer Printed Reflectarrays Using Patches of Variable Size', IEEE Transactions on Antennas and Propagation, vol. 49, no. 10, October 2001, pp. 1403-1410.

[8] J. A. Encinar, and J. A. Zornoza: 'Broadband Design of Three-Layer Printed Reflectarrays', IEEE Transactions on Antennas and Propagation, vol. 51, no. 7, 2003, pp. 1662-1664.
[9] E. Carasco, J. A. Encinar, and M. Barba: 'Bandwidth Improvement in Large Reflectarrays by Using True-Time Delay', IEEE Transactions on Antennas and Propagation, vol. 56, no. 8, 2008, pp. 2496-2503.
[10] M. R. Chaharmir, J. Shaker, M. Cuhaci, et al.: 'Broadband reflectarray antenna with double cross loops', Electronics Letters, vol. 42, no. 2, January 2006, pp. 65-66.
[11] M. R. Chaharmir and J. Shaker: 'Broadband reflectarray with combination of cross and rectangle loop elements', Electronics Letters, vol. 44, no. 11, May 2008, pp. 658-659.
[12] M. R. Chaharmir, J. Shaker, and H. Legay: 'Broadband Design of a Single Layer Large Reflectarray Using Multi Cross Loop Elements', IEEE Transactions on Antennas and Propagation, vol. 57, no. 10, October 2009, pp. 3363-3366.
[13] Q. Y. Chen, S. W. Qu, X. Q. Zhang, et al.: 'Low-Profile Wideband Reflectarray by Novel Elements with Linear Phase Response', IEEE Antennas and Wireless Propagation Letters, vol. 11, 2012, pp. 1545-1547.
[14] A. Vosoogh, K. Keyghobad, A. Khaleghi, et al.: 'A High-Efficiency Ku-Band Reflectarray Antenna Using Single-Layer Multiresonance Elements', IEEE Antennas and Wireless Propagation Letters, vol. 13, 2014, pp. 891-894.
[15] L. Moustafa, R. Gillard, F. Peris, et al.: 'The Phoenix Cell: A New Reflectarray Cell with Large Bandwidth and Rebirth Capabilities', IEEE Antennas and Wireless Propagation Letters, vol. 10, 2011, pp. 71-74.
[16] D. M. Pozar: 'Wideband reflectarrays using artificial impedance surfaces', Electronics Letters, vol. 43, no. 3, 2007 pp. 148–149.
[17] P. Nayeri, F. Yang, A. Z. Elsherbeni: 'A broadband microstrip reflectarray using sub-wavelength patch elements', IEEE Antennas and Propagation Society International Symposium, June 2009.
[18] G. Zhao, Y. C. Jiao, F. Zhang, et al.: 'A subwavelength element for broadband circularly polarized reflectarrays', IEEE Antennas and Propagation Letters, vol. 9, 2010, pp. 330–333.
[19] J. Ethier, M. R. Chaharmir, J. Shaker: 'Reflectarray design comprised of sub-wavelength coupled-resonant square loop elements', Electronics Letters, vol.47, no. 22, 2011, pp. 1215–1217.
[20] A. Edalati, and K. Sarabandi: 'Reflectarray antenna based on grounded loop-wire miniaturised-element frequency selective surfaces', IET Microwaves, Antennas & Propagation, vol. 8, no. 12, 2014, pp. 973-979.
[21] T. Makdissy R. Gillard, E. Fourn, et al.: 'A Patch-Slot Combination Approach for Large Band Reflectarrays', 42nd European Microwave Conference, Netherlands, 2012, pp. 759-762.